Synthesis, Characterization, and Reactivity of a Synthetic End-on Cobalt (II) Alkyl Persulfide Complex as a Model Platform for Thiolate Persulfidation

Keyan Li, Lev N. Zakharov, and Michael D. Pluth*

Department of Chemistry and Biochemistry, Materials Science Institute, Knight Campus for Accelerating Scientific Impact, and Institute of Molecular Biology, University of Oregon, Eugene, Oregon, 97403-1253, United States.

ABSTRACT: Persulfides (RSS^-) are ubiquitous source of sulfides (S^{2-}) in biology, and interactions between RSS^- and bioinorganic metal centers play critical roles in biological hydrogen sulfide (H_2S) biogenesis, signaling, and catabolism. Here we report the use of contact-ion stabilized [Na(15-crown-5)][^{t}BuSS] (**1**) as a simple synthon to access rare metal alkyl persulfide complexes and to investigate the reactivity of RSS^- with transition metal centers to provide insights into metal thiolate persulfidation including the fundamental difference between alkyl persulfides and alkyl thiolates. Reaction of **1** with $[Co^{II}(TPA)(OTf)]^+$ afforded the η^1-alkyl persulfide complex $[Co^{II}(TPA)(SS^tBu)]^+$ (**2**), which was characterized by X-ray crystallography, UV-vis spectroscopy, and Raman spectroscopy. RSS^- coordination to the Lewis acidic Co^{2+} center provided additional stability to the S–S bond as evidenced by a significant increase in the Raman stretching frequency for **2** (ν_{S-S} = 522 cm^{-1}, $\Delta\nu_{S-S}$ = 66 cm^{-1}). The effect of persulfidation on metal center redox potentials was further elucidated using cyclic voltammetry, in which the $Co^{2+} \rightarrow Co^{3+}$ oxidation potential of 2 ($E^{p,a}$ = +89 mV vs SCE) is lowered by nearly 700 mV when compared to the corresponding thiolate complex $[Co^{II}(TPA)(S^tBu)]^+$ (**3**) ($E^{p,a}$ = +818 mV vs SCE), despite persulfidation being an oxidative post-translational modification. Reactivity of 2 toward reducing agents including PPh_3, BH_4^-, and biologically relevant thiol reductant DTT led to different S^{2-} output pathways including formation of a dinuclear 2Co-2SH complex $[Co^{II}_2(TPA)_2(\mu^2\text{-}SH)_2]^{2+}$(**4**).

Introduction

Hydrogen sulfide (H_2S) plays vital roles in biology and is metabolized by most organisms ranging from bacteria and archaea to plants and mammals.[1] Despite its known toxicity, endogenous H_2S plays essential regulatory roles in complex physiological processes including vasodilation, neural transduction, and inflammation, joining nitric oxide (NO) and carbon monoxide (CO) as the third established gasotransmitter.[2] Recognition of the broad biological significance of H_2S has led to the rapid development of chemical tools for delivery and detection of H_2S and its related reactive sulfur species (RSS).[3] In addition to the biological roles of H_2S in eukaryotic organisms, specialized prokaryotes living in sulfur-rich environments have long used sulfides (S^{2-}) as their main energy sources, and multi-electron oxidation of S^{2-} to sulfate (SO_4^{2-}) remains one of the major reactions in the global sulfur cycle.[4]

Regulation of biological H_2S levels in most organisms involves the intermediacy of persulfides (RSS^-), which are typically in the form of post-translationally modified cysteine/glutathione residues bearing an additional sulfur atom in the –1 oxidation state.[5-7] RSS^- are often reductant-labile sources of biological S^{2-} and have been widely implicated in mammalian H_2S biogenesis by 3-mercaptopyruvatesulfurtransferase (3-MST) and also in the biosynthesis of essential S-containing cofactors including thiamin and molybdopterin.[8-11] Moreover, RSS^- production, utilization, and regulation are often intertwined with bioinorganic metal centers (Figure 1).[12] Most notably, iron-sulfur (Fe–S) cluster construction by the scaffold protein ISCU involves transfer of cysteine persulfides ($^{Cys}SS^-$) from cysteine desulfurase (IscS), and the exact mechanism of RSS^- reduction to S^{2-} and eventual [2Fe-2S] cluster formation remains an active area of study.[13-15] Furthermore, persulfidation from cysteine thiolates mediated by both redox-active and redox-inactive metal centers has been observed in tetraprolin (TPP),[16] ZnCu superoxide dismutase (SOD),[17-18] cysteine dioxygenase (CDO),[19] NiFe hydrogenases,[20-21] and other iron-sulfur (Fe–S) cofactors during assembly/disassembly.[22-24] Sulfide detoxification is of paramount importance in mammals and is mainly achieved by persulfide dioxygenase (ETHE1), which is a non-heme iron-dependent oxygenase that catalyzes oxygenation of glutathione persulfide (GSS^-) to sulfite (SO_3^{2-}).[25-27] The proposed mechanism involves initial end-on binding of GSS^- to the mononuclear Fe^{II} site, although the crystal structure of substrate-bound ETHE1 remains elusive due to the poor stability of persulfide-bound species.[28] Furthermore, interactions of RSS^- with metalloenzymes have also been observed in numerous sulfur-oxidizing bacteria and archaea that utilize Mo,[29] heme,[30-31] and non-heme

Fe[32-33] containing enzymes to catalyze the oxygenation of RSS^- to SO_3^{2-} to provide additional electrons for carbon fixation and respiration. Despite the biochemical significance of RSS^-, close examination of RSS^- and bioinorganic metal centers have often been hampered by the poor stability of RSS^-. The vital biological roles of RSS^- and the associated complex reaction pathways with biological metal ions highlight both the need and opportunity for rational synthetic strategies to access RSS^- containing model complexes to elucidate the spectroscopy, electronic structures, and biologically relevant reactivity of RSS^- containing metalloenzymes.

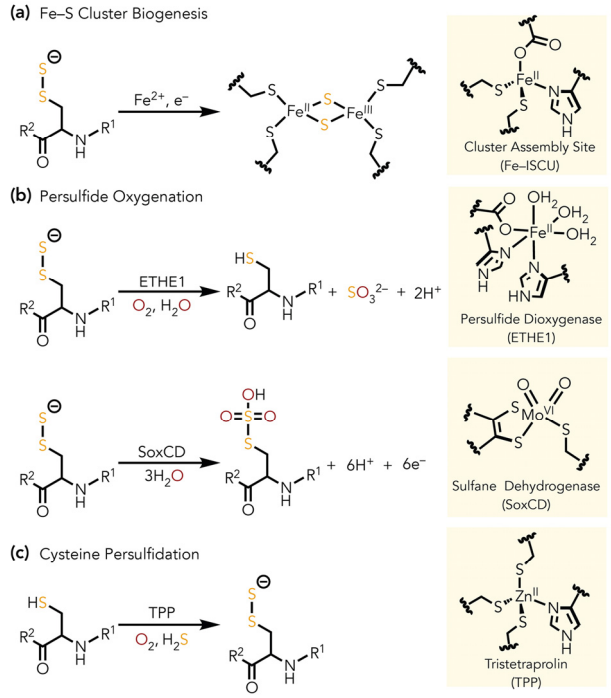

Figure 1. Selected examples of persulfide interaction with bioinorganic metal centers. (a) Fe-S cluster biogenesis from persulfides, (b) Oxygenation of persulfides by ETHE1 and SoxCD, (c) O_2 assisted persulfidation at TPP.

The wide redox availability of sulfur and highly complex interconversions between different reactive sulfur species through both one and two-electron mechanisms pose both opportunities and challenges for understanding the reactivity of RSS^-. Despite the prevalence of RSS^- in biology, synthetic systems of free RSS^- anions or those ligated to metal centers are scarce due to the high lability of RSS^-, which equilibrate with longer chain alkyl polysulfides ($RSSS_n^-$), polysulfide radicals ($S_3^{\cdot-}$), and disulfides (R_2S_2) in solution, further exacerbating modeling direct interactions between RSS^- and transition metal centers.[34-37] In addition, direct generation of metal alkyl persulfides complexes from metal thiolates and elemental sulfur (S_8) remains an inaccessible synthetic pathway, often yielding transition metal alkyl polysulfides and one-electron oxidized transition metal polysulfides.[38-39] Reported transition metal persulfide complexes have primarily generated as side-products and targeted syntheses are largely reliant on both the identities of metal centers and the associated primary coordination spheres.[40-41] To our knowledge, there are only three structurally characterized mononuclear alkyl persulfide complexes of late first-row transition metals (Figure 2). Kovacs and co-workers reported the first structurally characterized examples of late first-row transition metal η^2-alkyl persulfide complexes $[Fe^{III}(S^{Me2}N_3(Et,Pr)(\eta^2\text{-}S_2)][PF_6]$ through outer sphere oxidation of the corresponding thiolate complexes with $FcPF_6$.[42] Potenza and co-workers reported the first η^1-alkyl persulfide ligated Cu^{II} complex Cu^{II}(tet-b)$SSCH_2CO_2$ in an attempt to prepare the corresponding Cu^{II} thiolate relevant to the blue copper protein.[43] As a final example, Artaud and co-workers have prepared the first examples of RSS^- ligated Zn^{II} complexes using the basic hydroxo moiety of $TpZn^{II}OH$ (Tp: trispyrazolborate) to deprotonate sterically protected Ph_3CSSH and ^{t}BuSSH.[44] The role of basic hydroxo group within the primary coordination sphere proved essential to the successful isolation of RSS^- ligated species, although extension of this approach to other scaffolds has not been reported. Herein, we report a rational strategy for the syntheses of traditionally poorly accessible alkyl persulfide complexes using contact-ion stabilized RSS^- and describe the implications for thiolate persulfidation.

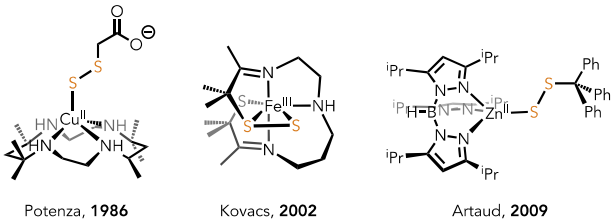

Figure 2. Selected examples of structurally characterized alkyl persulfide complexes of late first-row transition metals.

Results and Discussion

Syntheses and Characterization of Alkyl Persulfide Complexes.

Prior work in our group demonstrated that reactive alkyl dichalcogenide anions function as discrete, isolable motifs when complexed to $[K(18\text{-crown-6})]^+$.[45] Extending on this work, we prepared the more sterically encumbered $[^t\text{BuSS}]^-$ complexed to $[Na(15\text{-crown-5})]^+$ following similar procedures as a synthon for metal alkyl persulfide complexes (Scheme 1). Pre-complexation of NaS^tBu with 15-crown-5 in MeCN followed by the addition of S_8 afforded [Na(15-crown-5)][^{t}BuSS] (**1**), which exhibits no observable equilibration with higher-order polysulfides in solution by ^{1}H NMR spectroscopy or UV-vis spectroscopy unlike previously reported $[PPh_4][^t\text{BuSS}]$ (Figures S1, S20). The UV-vis spectrum of **1** reveals a single absorption band at λ_{max} = 369 nm corresponding to the nb → σ* transition, comparable to previously reported [K(18-crown-6)][BnSS] (λ_{max} = 373 nm).

Scheme 1. (a) Synthesis of alkyl persulfide precursor **1**. (b) Preparation of alkyl persulfide complex **2**.

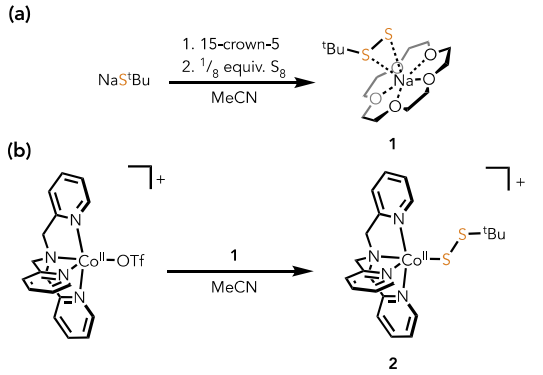

To test our hypothesis that alkali metal complexed RSS$^-$ can be used to access M–SSR complexes, we initially monitored the reaction between [Co^{II}(TPA)(OTf)][OTf] and **1** in MeCN by UV-vis, which generated new distinct absorption bands at λ_{max} = 506 nm and 635 nm corresponding to S → Co^{2+} charge transfer (CT) and spin-allowed *d*-*d* transition, respectively (Figure 3a). Repeating this reaction on a synthetic scale at –35 °C afforded [Co^{II}(TPA)(SS^{t}Bu)][OTf] (**2**·OTf), which was then treated with NaBPh$_4$ to afforded dark purple compound [Co^{II}(TPA)(SS^{t}Bu)][BPh$_4$] (**2**·BPh$_4$). Alkyl persulfide complex **2** is stable in the solid state under inert conditions for days but gradually decomposes into the corresponding thiolate [Co^{II}(TPA)(S^{t}Bu)]$^+$ (**3**) in solution. We used the Evans method to determine solution magnetic susceptibility values of μ_{eff}= 4.02 μ_B for **2** and μ_{eff}= 4.10 μ_B for **3**, both supportting high spin $S = {}^3/_2$ Co^{II} centers in a trigonal bipyramidal coordination environment. The ^{1}H NMR spectrum of **2** in CD$_3$CN in the paramagnetic region shows drastically shifted pyridyl C*H* (α_{C-H}: 130.6 ppm, β_{C-H}: 55.0 ppm, 49.4 ppm) and methylene C*H*$_2$ (100.5 ppm) resonances when compared to those of the parent compound [Co^{II}(TPA)(OTf)][OTf] (Figures S4-S5). In addition, a new broadened singlet at 8.69 ppm was observed corresponding to the ^{t}BuC*H*$_3$ proton resonance of **2**, which is shifted far upfield compared to the ^{t}BuC*H*$_3$ proton resonance of **2** (34.95 ppm), indicating that the ^{t}BuC*H*$_3$ protons are weakly associated with the paramagnetic center of **2**. The UV-vis spectrum of **2** in CH$_2$Cl$_2$ features a *d*-*d* transition at λ_{max} = 638 nm, which is slightly blue-shifted from the related feature of **3** at λ_{max} = 648 nm (Figures S22, S24).

To further understand the effect of coordination of RSS$^-$ to Lewis acidic metal centers, we investigated the electronic environment of S–S bonds in **1** and **2** using confocal Raman spectroscopy and observed sharp Raman peaks in the S–S stretching region at 456 cm^{-1} and 522 cm^{-1} for **1** and **2**, respectively (Figure 3b). The observed difference in vibrational frequency between **1** and **2** is consistent with our hypothesis that coordination of RSS$^-$ to Lewis-acidic Co^{2+} alleviates lone-pair repulsion between the terminal and internal S atoms, which results in strengthening of the S–S bonds in the coordinated RSS$^-$. Surprisingly, Raman spectroscopic features for biological or synthetic RSS$^-$ are scarce in present literature, and the sole example of RSS$^-$ characterized by Raman spectroscopy to our knowledge is [Fe$_2$S$_2$(^{Cys}S)$_2$(^{Cys}SS)$_2$]$^{2-}$ found in the O$_2$-sensing fumarate nitrate regulator (FNR) with ν_{S-S} = 498 cm^{-1}.[23]

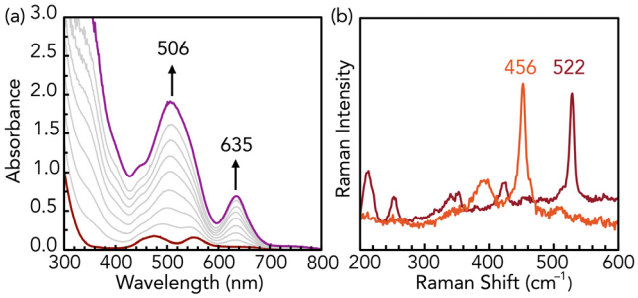

Figure 3. (a) UV-vis trace of the reaction between [Co^{II}(TPA)(OTf)][OTf] (red trace) and 0 – 1.6 equiv. [Na(15-crown-5)][SS^{t}Bu] in MeCN at room temperature to afford **2**·OTf. (b) Confocal Raman spectra of single crystals of **1** (orange trace) and **2** (red trace).

We further confirmed the structure of persulfide ligated **2**·BPh$_4$ using X-ray crystallography (Figure 4). Red-purple crystals suitable for X-ray diffraction were obtained from layering a saturated solution of **2**·BPh$_4$ in CH$_2$Cl$_2$ with hexanes and storing at –35 °C for 2 weeks. The geometry of **2**·BPh$_4$ is trigonal bipyramidal, similar to the corresponding thiolate complex **3**·BPh$_4$ and other reported five-coordinate Co^{II} TPA complexes. The presence of one anionic ^{t}BuSS$^-$ ligand and one BPh$_4^-$ counterion (per Co) further supports cobalt in the Co(II) oxidation state. The coordination mode of the ^{t}BuSS$^-$ ligand is best described as a monodentate η^1-alkyl persulfide with Co–S(1) and Co–S(2) of 2.311(2) Å and 3.312(3) Å, respectively. The S(1)–S(2) bond distance for **2**·BPh$_4$ is 2.087(4), which is similar to other reported η^1-alkyl persulfide complexes but shorter than the only reported first-row transition metal η^2-alkyl persulfide complex [Fe^{III}(S^{Me2}N$_3$(Et,Pr)(η^2-S$_2$)][PF$_6$].[42-44] Alkyl persulfide **2**·BPh$_4$ and thiolate **3**·BPh$_4$ share similar structural features as evidenced by minor differences in Co–S(1) distances (2.288(1) Å for **3**·BPh$_4$ vs. 2.311(2) Å for **2**·BPh$_4$) and Co–N(1) distances (2.256(3) Å for **3**·BPh$_4$ vs. 2.224(6) Å for **2**·BPh$_4$). To the best of our knowledge, **2**·BPh$_4$ is the first η^1-alkyl persulfide complex for Co.

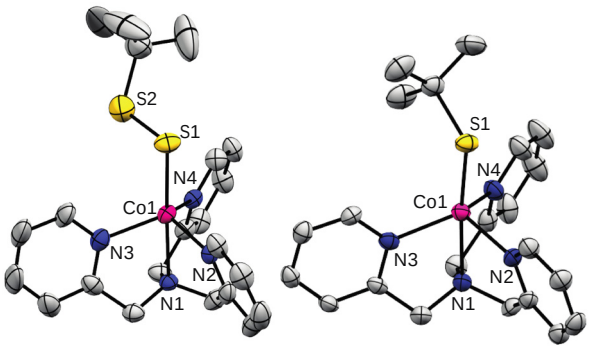

Figure 4. Solid-state structures of **2**·BPh$_4$ and **3**·BPh$_4$. Magenta, blue, yellow, and gray ellipsoids represent Co, N, S, and C atoms, respectively. Ellipsoids are shown at the 50% probability level. Counterions and H atoms are omitted for clarity.

We also investigated the effect of thiolate persulfidation on the redox potential of the metal centers by performing cyclic voltammetry (CV) experiments on both persulfide **2** and thiolate **3** (Figure 5). The CV of thiolate **3** in the –1.0 to

+1.0 V potential range revealed both oxidation of $Co^{2+} \rightarrow Co^{3+}$ ($E^{p,a}$ = +818 mV vs SCE) and subsequent reduction of $Co^{3+} \rightarrow Co^{2+}$ ($E^{p,c}$ = –289 mV vs SCE). The large peak-to-peak separation is consistent with previously reported five-coordinate Co^{II} thiolate complex $[Co^{II}(S^{Me2}N_4\text{-(tren)}]^+$ ($E^{p,a}$ = +270 mV vs SCE, $E^{p,c}$ = –729 mV vs SCE) by Kovacs and co-workers, in which electrochemical oxidation of $Co^{2+} \rightarrow Co^{3+}$ yields a stable solvent-bound six-coordinate species in solution.[46] Similar irreversible redox behaviors were observed in the CV of persulfide-ligated **2**, but we did observe a significant anodic shift for both oxidation event of $Co^{2+} \rightarrow Co^{3+}$ ($E^{p,a}$ = +89 mV vs SCE) and subsequent reduction event of $Co^{3+} \rightarrow Co^{2+}$ ($E^{p,c}$ = –896 mV vs SCE). These results suggest that thiolate persulfidation provides additional stability to metal centers in higher oxidation states that may prove significant for sulfide catabolism through S-oxygenation.

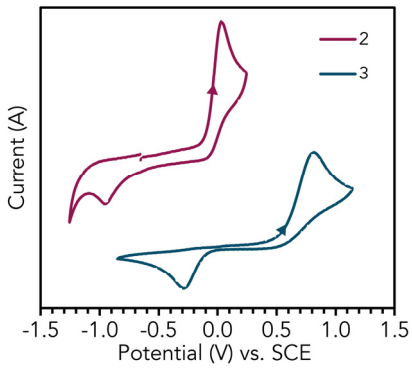

Figure 5. Cyclic voltammograms of **2**·BPh_4 (purple trace) and **3**·OTf (teal trace) in a solution of 0.3 M $[NBu_4][PF_6]$ in MeCN with an 100 mV/s scan rate.

Having established the impact of persulfide coordination on the redox potential of the metal, we also investigated the redox behavior of anionic persulfide **1**. Biological RSS^- can undergo facile one-electron oxidation to generate resonance-stabilized perthiyl radicals ($RSS^\bullet$) or one-electron reduction to form highly reactive alkyl persulfide radical anions ($RSSH^{\bullet-}/RSS^{\bullet 2-}$).[47-49] When analyzing the CV of **1**, we observed an irreversible oxidation event at –214 mV, which we attribute to formation of the unstable perthiyl radical (Figure S34). This peak oxidation potential is more anodic than HS^- oxidation ($E^{p,a}$ = +35 mV vs SCE for $[NBu_4][SH]$ in MeCN),[50] and is consistent with previously reported oxidation potential difference between biological RSS^- and HS^- (ΔE^{ox} = ~ 0.23 V).[51] In addition, coordination of RSS^- to Co^{2+} center further shifts $RSS^-/RSS^\bullet$ oxidation event toward more cathodic direction as anticipated, where the CV of **2** with wider potential range revealed a second irreversible oxidation event at +670 mV (Figure S36). Upon electrochemical reduction, we did not observe any notable reduction features in the CV of **1**, suggesting reduction of free RSS^- to S^{2-} and RS^- occurs at highly reducing and inaccessible potentials (Figure S35). The RSS^- reduction, however, does become accessible once coordinated to Co^{2+} based on the two irreversible reduction features emerged in the CV for **2** at –1420 mV and –1630 mV assigned to RSS^- and $Co^{2+/1+}$ reduction events, respectively.

Building from the spectroscopic, structural, and redox properties of **2**, we next investigated the fundamental reactivity of this alkyl persulfide complex with simple chemical reductants. To test whether metal-bound RSS^- can produce HS^-/S^{2-}, we treated **2** with two-electron reductant PPh_3, $[NBu_4][BH_4]$, and also the common disulfide reducing agent dithiothreitol (DTT) (Figure 6). Treatment of **2** in CD_3CN with PPh_3 resulted in formation of S^{2-} in the form of $S{=}PPh_3$ ($\delta(^{31}P)$ = 42 ppm) and the corresponding thiolate complex **3** was observed by ^{31}P and ^1H NMR spectroscopy (Figures S12-S13.) Upon treating **2** with $[NBu_4][BH_4]$ in MeCN, we observed the consumption of BH_4^-, formation of thiolate **3**, and liberation of HS^- (Figure S14). To further verify HS^- formation, treatment with BnBr resulted in BnSH and Bn_2S_2 formation (Figure S15), whereas treatment with PPh_3 failed to generate $S{=}PPh_3$, which further confirmed complete reduction of RSS^- to HS^- by $[NBu_4][BH_4]$ (Figure S16). Treatment of **2** with DTT, however, resulted in different product formation, and we observed disulfide (DTT_{ox}), ^{t}BuSH, and a new paramagnetic species by ^1H NMR spectroscopy and UV-vis spectroscopy with characteristic absorbances at 347 nm, 466 nm, 521 nm, and 633 nm (Figures S17, S18, S28). Because free RSS^- can release HS^- upon reduction by thiols, we also performed a control experiment between $[Co^{II}(TPA)(OTf)][OTf]$ and $[NBu_4][SH]$ in MeOH, which generated a new green species with identical ^1H NMR and UV-vis spectroscopic features (Figure S9, S27). The identity of this product was further determined by X-ray crystallography to be $[Co^{II}_2(TPA)_2(\mu^2\text{-}SH)_2][OTf]_2$ (**4**) (Figure 6b). Although crystallized as a dimer, hydrosulfide **4** is monomeric $[Co^{II}(TPA)_2(SH)]^+$ in solution as evidenced by ^1H NMR spectroscopy and a solution magnetic susceptivity of μ_{eff}= 4.01 μ_B (Figure S17). The reductive reactivity is consistent with our prior observations with free RSS^- anion and suggests that metal-bound RSS^- can also serve as reservoirs of S^{2-}.

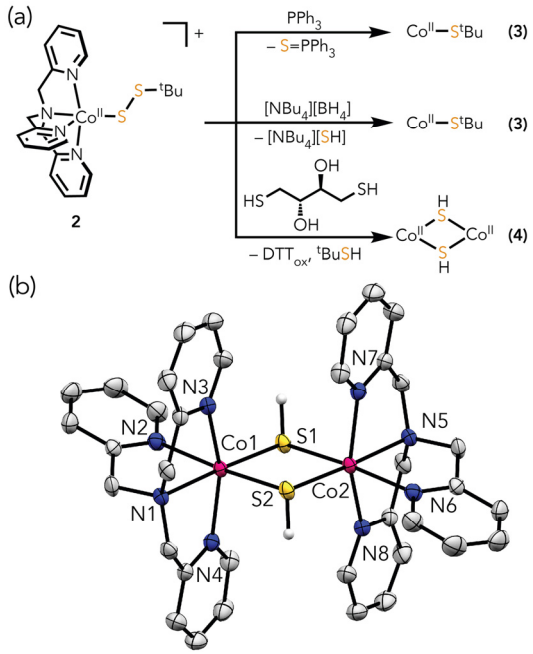

Figure 6. (a) Reductive reactivity of alkyl persulfide complexes toward PPh_3, $[NBu_4][BH_4]$ and dithiothreitol (DTT) (DTT_{ox}: *trans*-4,5-Dihydroxy-1,2-dithiane). (b) Solid-state structures of **4**. Magenta, blue, yellow, and gray ellipsoids represent Co, N, S, and C atoms, respectively. Ellipsoids are shown at the 50%

probability level. Counterions and H atoms are omitted for clarity.

Conclusion

We have described a rational strategy to directly probe the reactivity between transition metal centers and RSS^- relevant to cysteine posttranslational modification. The reaction between $[Na(15\text{-crown-}5)]^+$ stabilized RSS^- enabled the synthesis of the first end-on Co^{II} alkyl persulfide complex, which provided insights into metal thiolate persulfidation including the fundamental differences between alkyl persulfides and alkyl thiolates. Furthermore, we have demonstrated that this simple synthetic strategy can yield new model platforms for future reactivity studies including the reduction chemistry from RSS^- to S^{2-} relevant to Fe–S cluster biogenesis, O_2 activation chemistry relevant to biological sulfide catabolism by ETHE1, and other metalloenzyme-mediated chemical transformations relevant to the global sulfur cycle. We anticipate that this approach will be a fruitful path from which to investigate other metal alkyl persulfide motifs that have previously been inaccessible.

Experimental Section

Materials and Methods. All manipulations were carried out in an Inert Atmospheres nitrogen-filled glove box unless otherwise noted. Chemicals were purchased from TCI, Sigma Aldrich, VWR International, Acros, Alpha Aesar, or Cambridge Isotopes. Molecular sieves (4 Å) and Celite® were activated by heating to 300 °C under vacuum and were stored under N_2. Bulk solvents were deoxygenated and dried by sparging with argon gas followed by passage through an activated alumina column in a Pure Process Technologies solvent system. Solvents are stored over 4 Å sieves under a nitrogen atmosphere. Anhydrous and degassed MeOH was purchased from Thermo Fischer. CD_3CN was distilled over K_2CO_3 under N_2 and stored over activated 4 Å sieves prior to use. CD_2Cl_2 was distilled over CaH_2 and degassed through three freeze-pump-thaw cycles. NaSBn and NaS^{t}Bu were prepared by deprotonation of BnSH and ^{t}BuSH with NaH in THF, respectively. Previously reported $[Co^{II}(TPA)OTf][OTf]$ was prepared by stirring commercially available $CoOTf_2$ with TPA ligand in MeCN.[52] $[NBu_4][SH]$ and $[Co^{II}(TPA)Cl][Cl]$ were prepared following literature procedures,[50, 53] and salt metathesis reaction between $[Co^{II}(TPA)Cl][Cl]$ and $NaBPh_4$ in MeCN afforded $[Co^{II}(TPA)Cl][BPh_4]$ bearing identical UV-vis features and diagnostic paramagnetic ^{1}H NMR resonances of $[Co^{II}(TPA)Cl][Cl]$. UV/vis spectra were acquired on an Agilent Cary 60 UV/vis spectrophotometer equipped with a Quantum Northwest TC-1 temperature controller. NMR spectra were acquired on a Bruker Avance-III-HD 600 spectrometer (^{1}H: 600 MHz, ^{13}C: 151 MHz, ^{31}P: 242 MHz), Chemical shifts are reported in parts per million (δ) and referenced to residual protic solvent resonances. Mass spectrometry was performed by the Microanalytical Facility at University of Illinois Urbana-Champaign. IR spectra were acquired on a Nicolet 6700 IR Spectrometer as KBr pellet samples.

Confocal Raman Microscopy. Confocal Raman spectra were acquired on a Renishaw inVia confocal Raman microscope. Optimal spectra of 1 and 2 were collected using a 50x objective lens with a 2400/mm grating and a 488 nm laser. The instrument was calibrated using a Si wafer prior to use. Air-sensitive microcrystalline samples 1 and 2 were prepared inside a glovebox, placed on a glass slide, coated with ParatoneN oil, and covered with a glass slide cover slip before removing from an inert atmosphere for further analysis.

Electrochemical Measurements. Cyclic voltammograms (CVs) were recorded in a nitrogen atmosphere using a Biologic SP-50 potentiostat with a glassy carbon working electrode, a platinum wire auxiliary electrode, and an $Ag/AgNO_3$ (0.001M) non-aqueous reference electrode. All potentials are referenced to the SCE couple, and ferrocene was used as an external standard where the E½ of ferrocene/ferrocenium is +0.40 V vs. SCE in 0.3 M $[Bu_4N][PF_6]$ MeCN. $[Bu_4N][PF_6]$ was recrystallized from ethanol and placed under vacuum for 72 hours at 85 °C before electrolyte solutions were made from anhydrous and Ar saturated MeCN.

X-ray Crystallography. Diffraction intensities were collected at 173 K (**3**·BPh_4 and **4**·$(OTf)_2$) and 223 K (**2**·BPh_4) on Rigaku Synergy-S and Bruker Apex2 single crystal diffractometers using CuK_α (**3**·BPh_4) and MoK_α (**2**·BPh_4 and **4**·$(OTf)_2$) radiation, 1.54178 Å and 0.71073 Å respectively. Space groups were determined based on systematic absences. Absorption corrections were applied by SADABS.[54] Structures were solved by direct methods and Fourier techniques and refined on F^2 using full matrix least-squares procedures. All non-H atoms were refined with anisotropic thermal parameters. H atoms in **2**·BPh_4 and **4**·$(OTf)_2$ were refined in calculated positions in a rigid group model except the H atom at the S atom in **4**·$(OTf)_2$. The –SH- bridge in **4**·$(OTf)_2$ is disordered over two positions with opposite orientations. The H atom at the S atom in both disordered positions were found on the residual density map but it was refined with restrictions: the standard S-H distance of 1.34 Å was used as the target for the S-H bonds in both positions. H atoms in **3**·BPh_4 were found on the residual density map and refined with isotropic thermal parameters. Solvent molecules (CH_2Cl_2 in **2**·BPh_4 and CH_3OH in **4**·$(OTf)_2$) are highly disordered and were treated by SQUEEZE.[55] Crystals of **2**·BPh_4 are formed as twins consisting of two domains with significant overlapping for X-ray reflections. The structure of **2**·BPh_4 was determined and refined based on the HKLF4 set only. However, it provides an appropriate ratio of the number of the measured reflections per the number of the refined parameters 6947/487. The refinement of this structure based on the HKLF5 set did not improve the final results. All calculations were performed by the Bruker SHELXL-2014/7 package.[56]

Syntheses of Compounds.

[Na(15-crown-5)][^{t}BuSS] (**1**). A solution of 15-crown-5 (353 mg, 1.60 mmol) in MeCN (1 mL) was added to a stirring suspension of NaS^{t}Bu (150 mg, 1.33 mmol) in MeCN (1 mL) to yield a clear reaction mixture. Solid S_8 (34.3 mg, 1.07 mmol) was added to the reaction mixture turning the initially clear solution to teal green. The reaction mixture was stirred for 2 h to yield a homogenous yellow solution, which was filtered through a pad of Celite. The resulting pale-yellow filtrate was concentrated under reduced pressure to a quarter of its original volume and was layered with excess Et_2O. Storing this mixture at –35 °C overnight gave an off-

white crystalline solid, which was collected by decanting the supernatant followed by drying under reduced pressure (202 mg, 44 %). ^{1}H NMR (600 MHz, CD_3CN): δ 3.64 (s, 20H, 15-crown-5), 1.20 (s, 9H, C(CH_3)$_3$). ^{13}C{^{1}H} NMR (151 MHz, CD_3CN): 69.6, 41.8, 29.8. UV–vis in CH_3CN λ_{max} (ε_M, $M^{-1}cm^{-1}$): 345 (1402), 521 (822), 638 (405). UV–vis in CH_3CN λ_{max} (ε_M, $M^{-1}cm^{-1}$): 369 (524).

[Co^{II}(TPA)(SS^{t}Bu)][BPh$_4$](**2**·BPh_4). Separate solutions of [Co^{II}(TPA)(OTf)][OTf] (177 mg, 0.267 mmol) in a MeCN : THF (1:1) solvent mixture (10 mL) and **1** (100 mg, 0.294 mmol) in THF (2 mL) were cooled to –35 °C in the freezer for at least 15 min. Cold solution of **1** was then added dropwise to the stirring solution of [Co^{II}(TPA)OTf][OTf] during which the initially dark red solution turned maroon purple. The reaction mixture was allowed to stir for 2 h at room temperature before filtration through a pad of Celite. Volatiles from the dark purple filtrate was removed *in vacuo* to give a purple solid, which was washed with excess cold MeOH followed by drying under reduced pressure to give a brownish purple powder containing desired complex **2**·BPh_4 and minor byproduct **3**·BPh_4. The crude product was redissolved in minimal cold MeCN, layered with excess Et_2O, and held at –35 °C to give microcrystalline dark purple solids, which was collected through filtration. Dark purple crystalline plates suitable for X-ray diffraction were obtained by layering minimal hexanes onto a saturated solution of **2**·BPh_4 in CH_2Cl_2 held at –35 °C for 2 weeks (70 mg, 33 %). ^{1}H NMR (600 MHz, CD_3CN): δ 130.55, 100.50, 55.03, 49.41, 8.69, 7.36, 6.96, 6.77. –0.65. UV–vis in CH_2Cl_2 λ_{max} (ε_M, $M^{-1}cm^{-1}$): 345 (1402), 521 (822), 638 (405). HRMS (ESI) m/z [M]$^+$ calcd for $[C_{22}H_{27}CoN_4S_2]^+$: 470.1009; found: 470.1180. Evan's Method (CH_2Cl_2): μ_{eff}= 4.02 μ_B at 298K

[Co^{II}(TPA)(SS^{t}Bu)][OTf](**2**·OTf). [Co^{II}(TPA)(OTf)][OTf] (192 mg, 0.290 mmol) was dissolved in MeCN (5 mL) to give a purple solution, and this mixture was cooled to –35 °C in the freezer for 15 min. A separate chilled solution of **1** (109 mg, 0.312 mmol) was added dropwise turning the initially dark red solution to an intense maroon purple solution. The resulting mixture was allowed to stir for 10 min before volatiles were removed *in vacuo* to give a sticky residue. The crude product was extracted into chilled fluorobenzene before filtering through a pad of Celite to remove salt byproducts. Volatiles were removed and the resulting solids were washed with hexanes to removed 15-crown-5. The resulting product was recrystallized from layering Et_2O over a saturated solution of the crude material in MeCN to give purple crystalline solids overnight (78 mg, 43%). Diagnostic UV-vis and ^{1}H NMR spectroscopic features for **2**·OTf are consistent with **2**·BPh_4.

[Co^{II}(TPA)(S^{t}Bu)][BPh$_4$](**3**·BPh_4). [Co^{II}(TPA)Cl][BPh_4] (59 mg, 0.078 mmol) was dissolved MeCN (3 mL), and solid NaS^{t}Bu (9.2 mg, 0.082 mmol) was added. The reaction mixture was allowed to stir overnight, during which the initially teal green solution turned olive brown. The volatiles were removed *in vacuo*, and the resulting dark brown solids were extracted in minimal CH_2Cl_2. The resulting cloudy olive brown mixture was filtered through a Celite plug to remove salt byproducts and the dark olive-green filtrate was layered with minimal hexanes. Storing this mixture at –35 °C afforded yield crystalline dark olive brown plates suitable for X-ray diffraction (29 mg, 49%). ^{1}H NMR (600 MHz, CD_3CN): δ 117.71, 96.33, 54.33, 50.02, 34.95, 7.43, 6.95, 6.72. UV–vis in CH_2Cl_2 λ_{max} (ε_M, $M^{-1}cm^{-1}$): 344 (1331), 408 (1816), 460 (1344), 536 (230), 648 (406). HRMS (ESI) m/z [M]$^+$ calcd for $[C_{22}H_{27}CoN_4S]^+$: 438.1288; found: 438.1259. Evan's Method (CH_2Cl_2): μ_{eff}= 4.10 μ_B at 298K

[Co^{II}(TPA)(S^{t}Bu)][OTf](**3**·OTf). [Co^{II}(TPA)(OTf)][OTf] (50 mg, 0.076 mmol) and NaS^{t}Bu (8.5 mg, 0.076 mmol) was stirred in MeCN to give a dark olive green solution overnight. The volatiles were removed *in vacuo* and resulting solids were extracted in fluorobenzene then filtered through Celite to remove salt byproducts. Solvents were removed under reduced pressure, and crude product was extracted into minimal MeCN, layered with Et_2O, and stored in the freezer overnight to give dark brown crystals (12 mg, 27 %). Diagnostic UV-vis and ^{1}H NMR spectroscopic features for **3**·OTf are consistent with **3**·BPh_4.

[Co$^{II}_2$(TPA)$_2$(μ^2-SH)$_2$][OTf]$_2$ (**4**·$(OTf)_2$). [Co^{II}(TPA)(OTf)][OTf] (63 mg, 0.095 mmol) was dissolved in anhydrous MeOH (2 mL) and [NBu_4][SH] (5.6 mg, 0.10 mmol) in MeOH (1 mL) was added dropwise to the stirring solution, turning the initially red-orange solution to forest green. The reaction mixture was stirred for 10 min before filtering through a pipet filter, and the filtrate was concentrated to a third of its original volume. Layering excess Et2O over the concentrated filtrate followed by storing the mixture at –35 °C afforded red block crystals suitable for X-ray diffraction (11 mg, 22 %) ^{1}H NMR (600 MHz, CD_3CN): δ 116.51, 99.47, 57.28, 48.45, 7.43, 6.95, 6.72, –1.49. UV–vis in MeOH λ_{max} (ε_M, $M^{-1}cm^{-1}$): 344 (1801), 463 (269), 514 (264), 625 (319). Evan's Method (CH_2CN): μ_{eff}= 4.01 μ_B at 298K.

Reduction of **2** *by DTT*. Compound **2**·BPh_4 (17 mg, 0.021 mmol) was dissolved in CD_3CN (2 mL) in an NMR tube and DTT (3.3 mg, 0.021 mmol) was added. The reaction mixture was allowed to stand overnight, during which the reaction mixture turned from purple to a blackish color. The crude mixture was then analyzed by ^{1}H NMR spectroscopy to show the formation of DTT_{ox}, ^{t}BuSH, and **4**. (Figure S17-S18).

Reduction of **2** *by [NBu$_4$][BH$_4$]*. Compound **2**·OTf (10 mg, 0.016 mmol) was dissolved in MeCN (2 mL) and [NBu_4][BH_4] (5.0 mg, 0.018 mmol) in MeCN was added dropwise. The reaction mixture was allowed to stir overnight before solvents were removed under reduced pressure. The ^{1}H NMR spectrum of the crude reaction mixture showed full consumption of [NBu_4][BH_4] and did not reveal formation of **4** but rather of **3**. Treatment of the crude mixture with excess BnBr enabled trapping of HS^- as BnSH and Bn_2S, and treatment of the crude mixture with PPh_3 showed no formation of S=PPh_3 indicating full reduction of RSS^- to S^{2-}.(Figure S14-S16)

Reduction of **2** *by PPh$_3$*. A sample of **2**·BPh_4 (18.9 mg, 0.0237 mmol) in CD_3CN in an NMR tube was treated with PPh_3 (6.20 mg, 0.024 mmol) in CD_3CN. The tube was shaken vigorously during which the initially dark purple solution turned olive brown, consistent with the appearance of **3**. Subsequent analysis by ^{1}H and ^{31}P NMR spectroscopy revealed the formation of S=PPh_3 and **3**. (Figure S12-S13)

ASSOCIATED CONTENT

Supporting Information

Supporting Information. NMR spectra, UV-vis data, Raman spectra, crystallography details. This material is available free of charge via the Internet at http://pubs.acs.org.

AUTHOR INFORMATION

Corresponding Author

* pluth@uoregon.edu

ACKNOWLEDGMENT

We thank the NSF (CHE-2004150 to M. D. P., DGE-2022168 to K. L.) for support of this research. We also thank Prof. Shannon Boettcher and Prof. Michael Haley for the use of their potentiostats, Dr. Tobias Sherbow for helpful discussions, Nick D'Antona for assistance with electrochemical measurements, Golnaz Navidi and Dr. Lawrence Scatena for assistance with confocal Raman microscopy.

REFERENCES

(1) Kabil, O.; Banerjee, R., Redox Biochemistry of Hydrogen Sulfide. *J. Biol. Chem.* **2010,** *285*, 21903-21907.

(2) Wang, R., Two's Company, Three's a Crowd: Can H_2S Be the Third Endogenous Gaseous Transmitter? *FASEB J.* **2002,** *16*, 1792-1798.

(3) Fosnacht, K. G.; Pluth, M. D., Activity-Based Fluorescent Probes for Hydrogen Sulfide and Related Reactive Sulfur Species. *Chem. Rev.* **2024,** *124*, 4124-4257.

(4) Bamford, V. A.; Bruno, S.; Rasmussen, T.; Appia-Ayme, C.; Cheesman, M. R.; Berks, B. C.; Hemmings, A. M., Structural Basis for the Oxidation of Thiosulfate by a Sulfur Cycle Enzyme. *EMBO J.* **2002,** *21*, 5599-5610.

(5) Mishanina, T. V.; Libiad, M.; Banerjee, R., Biogenesis of Reactive Sulfur Species for Signaling by Hydrogen Sulfide Oxidation Pathways. *Nat Chem Biol* **2015,** *11*, 457-464.

(6) Lau, N.; Pluth, M. D., Reactive Sulfur Species (RSS): Persulfides, Polysulfides, Potential, and Problems. *Curr. Opin. Chem. Biol.* **2019,** *49*, 1-8.

(7) Fukuto, J. M.; Lin, J.; Khodade, V. S.; Toscano, J. P., Predicting the Possible Physiological/Biological Utility of the Hydropersulfide Functional Group Based on Its Chemistry: Similarities between Hydropersulfides and Selenols. *Antioxid. Redox Signal.* **2020,** *33*, 1295-1307.

(8) Lehmann, C.; Begley, T. P.; Ealick, S. E., Structure of the Escherichia Coli This−Thif Complex, a Key Component of the Sulfur Transfer System in Thiamin Biosynthesis. *Biochemistry* **2006,** *45*, 11-19.

(9) Matthies, A.; Nimtz, M.; Leimkühler, S., Molybdenum Cofactor Biosynthesis in Humans: Identification of a Persulfide Group in the Rhodanese-Like Domain of MOCS3 by Mass Spectrometry. *Biochemistry* **2005,** *44*, 7912-7920.

(10) Mueller, E. G., Trafficking in Persulfides: Delivering Sulfur in Biosynthetic Pathways. *Nat Chem Biol* **2006,** *2*, 185-194.

(11) Pedre, B.; Talwar, D.; Barayeu, U.; Schilling, D.; Luzarowski, M.; Sokolowski, M.; Glatt, S.; Dick, T. P., 3-Mercaptopyruvate Sulfur Transferase Is a Protein Persulfidase. *Nat Chem Biol* **2023,** *19*, 507-517.

(12) Fukuto, J. M.; Vega, V. S.; Works, C.; Lin, J., The Chemical Biology of Hydrogen Sulfide and Related Hydropersulfides: Interactions with Biologically Relevant Metals and Metalloproteins. *Curr. Opin. Chem. Biol.* **2020,** *55*, 52-58.

(13) Srour, B.; Gervason, S.; Hoock, M. H.; Monfort, B.; Want, K.; Larkem, D.; Trabelsi, N.; Landrot, G.; Zitolo, A.; Fonda, E., et al., Iron Insertion at the Assembly Site of the Iscu Scaffold Protein Is a Conserved Process Initiating Fe–S Cluster Biosynthesis. *J. Am. Chem. Soc.* **2022,** *144*, 17496-17515.

(14) Braymer, J. J.; Lill, R., Iron–Sulfur Cluster Biogenesis and Trafficking in Mitochondria. *J. Biol. Chem.* **2017,** *292*, 12754-12763.

(15) Zheng, L.; White, R. H.; Cash, V. L.; Dean, D. R., Mechanism for the Desulfurization of L-Cysteine Catalyzed by the Nifs Gene Product. *Biochemistry* **1994,** *33*, 4714-4720.

(16) Lange, M.; Ok, K.; Shimberg, G. D.; Bursac, B.; Markó, L.; Ivanović-Burmazović, I.; Michel, S. L. J.; Filipovic, M. R., Direct Zinc Finger Protein Persulfidation by H_2S Is Facilitated by Zn^{2+}. *Angew. Chem. Int .Ed.* **2019,** *58*, 7997-8001.

(17) Olson, K. R.; Gao, Y.; Arif, F.; Arora, K.; Patel, S.; DeLeon, E. R.; Sutton, T. R.; Feelisch, M.; Cortese-Krott, M. M.; Straub, K. D., Metabolism of Hydrogen Sulfide (H_2S) and Production of Reactive Sulfur Species (RSS) by Superoxide Dismutase. *Redox Biology* **2018,** *15*, 74-85.

(18) Switzer, C. H.; Kasamatsu, S.; Ihara, H.; Eaton, P., Sod1 Is an Essential H_2S Detoxifying Enzyme. *Proc. Natl. Acad. Sci.* **2023,** *120*, e2205044120.

(19) Souness, R. J.; Kleffmann, T.; Tchesnokov, E. P.; Wilbanks, S. M.; Jameson, G. B.; Jameson, G. N. L., Mechanistic Implications of Persulfenate and Persulfide Binding in the Active Site of Cysteine Dioxygenase. *Biochemistry* **2013,** *52*, 7606-7617.

(20) Volbeda, A.; Martin, L.; Barbier, E.; Gutiérrez-Sanz, O.; De Lacey, A. L.; Liebgott, P.-P.; Dementin, S.; Rousset, M.; Fontecilla-Camps, J. C., Crystallographic Studies of [NiFe]-Hydrogenase Mutants: Towards Consensus Structures for the Elusive Unready Oxidized States. *J Biol Inorg Chem* **2015,** *20*, 11-22.

(21) Marques, M. C.; Coelho, R.; Pereira, I. A. C.; Matias, P. M., Redox State-Dependent Changes in the Crystal Structure Of [NiFeSe] Hydrogenase from Desulfovibrio Vulgaris Hildenborough. *Int. J. Hydrogen Energy* **2013,** *38*, 8664-8682.

(22) Nicolet, Y.; Rohac, R.; Martin, L.; Fontecilla-Camps, J. C., X-Ray Snapshots of Possible Intermediates in the Time Course of Synthesis and Degradation of Protein-Bound Fe_4S_4 Clusters. *Proc. Natl. Acad. Sci.* **2013,** *110*, 7188-7192.

(23) Zhang, B.; Crack, J. C.; Subramanian, S.; Green, J.; Thomson, A. J.; Le Brun, N. E.; Johnson, M. K., Reversible Cycling between Cysteine Persulfide-Ligated [2Fe-2S] and Cysteine-Ligated [4Fe-4S] Clusters in the FNR Regulatory Protein. *Proc. Natl. Acad. Sci.* **2012,** *109*, 15734-15739.

(24) Aragão, D.; Macedo, S.; Mitchell, E. P.; Romão, C. V.; Liu, M. Y.; Frazão, C.; Saraiva, L. M.; Xavier, A. V.; LeGall, J.; van Dongen, W. M. A. M., et al., Reduced Hybrid Cluster Proteins (HCP) from Desulfovibrio Desulfuricans ATCC 27774 and Desulfovibrio Vulgaris (Hildenborough): X-Ray Structures at High Resolution Using Synchrotron Radiation. *J Biol Inorg Chem* **2003,** *8*, 540-548.

(25) Kabil, O.; Banerjee, R., Characterization of Patient Mutations in Human Persulfide Dioxygenase (ETHE1) Involved in H_2S Catabolism. *J. Biol. Chem.* **2012,** *287*, 44561-44567.

(26) Lin, B.; Ma, G.; Liu, Y., Mechanism of the Glutathione Persulfide Oxidation Process Catalyzed by Ethylmalonic Encephalopathy Protein. *ACS Catal.* **2016,** *6*, 7010-7020.

(27) Goudarzi, S.; Babicz, J. T., Jr.; Kabil, O.; Banerjee, R.; Solomon, E. I., Spectroscopic and Electronic Structure Study of ETHE1: Elucidating the Factors Influencing Sulfur Oxidation and Oxygenation in Mononuclear Nonheme Iron Enzymes. *J. Am. Chem. Soc.* **2018,** *140*, 14887-14902.

(28) Pettinati, I.; Brem, J.; McDonough, M. A.; Schofield, C. J., Crystal Structure of Human Persulfide Dioxygenase: Structural Basis of Ethylmalonic Encephalopathy. *Human Mol. Gen.* **2015,** *24*, 2458-2469.

(29) Zander, U.; Faust, A.; Klink, B. U.; de Sanctis, D.; Panjikar, S.; Quentmeier, A.; Bardischewsky, F.; Friedrich, C. G.; Scheidig, A. J., Structural Basis for the Oxidation of Protein-Bound Sulfur by the Sulfur Cycle Molybdohemo-Enzyme Sulfane Dehydrogenase SoxCD. *J. Biol. Chem.* **2011,** *286*, 8349-8360.

(30) Kappler, U.; Maher, M. J., The Bacterial Soxax Cytochromes. *Cell. Mol. Life Sci.* **2013,** *70*, 977-992.

(31) Dambe, T.; Quentmeier, A.; Rother, D.; Friedrich, C.; Scheidig, A. J., Structure of the Cytochrome Complex Soxxa of Paracoccus Pantotrophus, a Heme Enzyme Initiating Chemotrophic Sulfur Oxidation. *J. Structural. Biol.* **2005,** *152*, 229-234.

(32) Ferreira, P.; Fernandes, P. A.; Ramos, M. J., The Archaeal Non-Heme Iron-Containing Sulfur Oxygenase Reductase. *Coord. Chem. Rev.* **2022,** *455*, 214358.

(33) Sato, Y.; Yabuki, T.; Adachi, N.; Moriya, T.; Arakawa, T.; Kawasaki, M.; Yamada, C.; Senda, T.; Fushinobu, S.; Wakagi, T., Crystallographic and Cryogenic Electron Microscopic Structures and Enzymatic Characterization of Sulfur Oxygenase Reductase from *Sulfurisphaera Tokodaii*. *J. Structural Biol. X* **2020,** *4*, 100030.

(34) Jungen, S.; Paenurk, E.; Chen, P., Synthesis, Spectroscopic, and Structural Characterization of Organyl Disulfanides and a Tetrasulfanide. *Inorg. Chem.* **2020,** *59*, 12322-12336.

(35) Krautscheid, U.; Dev, S.; Krautscheid, H.; Paul, P. P.; Wilson, S. R.; Rauchfuss, T. B., N-Methylimidazole Mediated Chemistry of Transition Metal Phenylthiolates. The Isolation of the Perthiolate Salts $[M(N\text{-}Meim)_6](S_2Ph)_2$. *Z. Naturforsch.* **1993,** *48*, 653-658.

(36) Seo, W. T. M.; Riffel, M. N.; Oliver, A. G.; Tsui, E. Y., Metal-Cation-Induced Shifts in Thiolate Redox and Reduced Sulfur Speciation. *Chem. Sci.* **2024**.

(37) Kawamura, S.; Kitao, T.; Nakabayashi, T.; Horii, T.; Tsurugi, J., Aralkyl Hydrodisulfides. VIII. Alkaline Decomposition and Its Competition with Nucleophiles. *J. Org. Chem.* **1968,** *33*, 1179-1181.

(38) Ballesteros, M., II; Tsui, E. Y., Reactivity of Zinc Thiolate Bonds: Oxidative Organopolysulfide Formation and S_3 Insertion. *Inorg. Chem.* **2019,** *58*, 10501-10507.

(39) Atta, S.; Majumdar, A., Redox Convergent Synthesis and Reactivity of a Cobalt(III)-Pentasulfido Compound. *Chem. - Eur. J.* **2023,** *29*, e202203579.

(40) Shaver, A.; Hartgerink, J.; Lai, R. D.; Bird, P.; Ansari, N., Catenated Sulfur Ligands: The Synthesis of Metal Disulfanes and the Structures of cis-$(PPh_3)_2Pt(L)SSCHMe_2$ (L = Phthalimido) and $(Eta5\text{-}C_5h_5)W(CO)_3ssc_6h_4me$-P. *Organometallics* **1983,** *2*, 938-940.

(41) Galardon, E.; Deschamps, P.; Tomas, A.; Roussel, P.; Artaud, I., An Alternate Route to Disulfanido Complexes by Nucleophilic Attack of Thiolates on Ruthenium-Bound Thiosulfonato Ligands. *Inorg. Chem.* **2010,** *49*, 9119-9121.

(42) Schweitzer, D.; Shearer, J.; Rittenberg, D. K.; Shoner, S. C.; Ellison, J. J.; Loloee, R.; Lovell, S.; Barnhart, D.; Kovacs, J. A., Enhancing Reactivity via Structural Distortion. *Inorg. Chem.* **2002,** *41*, 3128-3136.

(43) John, E.; Bharadwaj, P. K.; Krogh-Jespersen, K.; Potenza, J. A.; Schugar, H. J., Molecular and Electronic Structure of Cu(Tet-B)$Ssch_2co_2.3ch_3oh$, a Novel Copper(II) Alkyl Persulfide Complex. *J. Am. Chem. Soc.* **1986,** *108*, 5015-5017.

(44) Galardon, E.; Tomas, A.; Selkti, M.; Roussel, P.; Artaud, I., Synthesis, Characterization, and Reactivity of Alkyldisulfanido Zinc Complexes. *Inorg. Chem.* **2009,** *48*, 5921-5927.

(45) Li, K.; Zakharov, L. N.; Pluth, M. D., Taming the Dichalcogenides: Isolation, Characterization, and Reactivity of Elusive Perselenide, Persulfide, Thioselenide, and Selenosulfide Anions. *J. Am. Chem. Soc.* **2023,** *145*, 13435-13443.

(46) Brines, L. M.; Shearer, J.; Fender, J. K.; Schweitzer, D.; Shoner, S. C.; Barnhart, D.; Kaminsky, W.; Lovell, S.; Kovacs, J. A., Periodic Trends within a Series of Five-Coordinate Thiolate-Ligated $[M^{ii}(Sme_2n_4(Tren))]^+$ (M = Mn, Fe, Co, Ni, Cu, Zn) Complexes, Including a Rare Example of a Stable Cu^{ii}–Thiolate. *Inorg. Chem.* **2007,** *46*, 9267-9277.

(47) Everett, S. A.; Wardman, P., [5] Perthiols as Antioxidants: Radical-Scavenging Andprooxidative Mechanisms. In *Methods in Enzymology*, Academic Press: 1995; Vol. 251, pp 55-69.

(48) Everett, S. A.; Folkes, L. K.; Wardman, P.; Asmus, K. D., Free-Radical Repair by a Novel Perthiol: Reversible Hydrogen Transfer and Perthiyl Radical Formation. *Free Radical Res.* **1994,** *20*, 387-400.

(49) Filipovic, M. R.; Zivanovic, J.; Alvarez, B.; Banerjee, R., Chemical Biology of H_2S Signaling through Persulfidation. *Chem. Rev.* **2018,** *118*, 1253-1337.

(50) Hartle, M. D.; Meininger, D. J.; Zakharov, L. N.; Tonzetich, Z. J.; Pluth, M. D., Nbu_4sh Provides a Convenient Source of HS^- Soluble in Organic Solution for H_2S and Anion-Binding Research. *Dalton Trans.* **2015,** *44*, 19782-19785.

(51) Benchoam, D.; Cuevasanta, E.; Möller, M. N.; Alvarez, B., Hydrogen Sulfide and Persulfides Oxidation by Biologically Relevant Oxidizing Species. *Antioxidants* **2019,** *8*, 48.

(52) Ward, A. L.; Elbaz, L.; Kerr, J. B.; Arnold, J., Nonprecious Metal Catalysts for Fuel Cell Applications: Electrochemical Dioxygen Activation by a Series of First Row Transition Metal Tris(2-Pyridylmethyl)Amine Complexes. *Inorg. Chem.* **2012,** *51*, 4694-4706.

(53) Chan, S. L.-F.; Lam, T. L.; Yang, C.; Lai, J.; Cao, B.; Zhou, Z.; Zhu, Q., Cobalt(II) Tris(2-Pyridylmethyl)Amine Complexes $[Co(Tpa)X]^+$ Bearing Coordinating Anion ($X=Cl^-$, Br^-, I^- and NCS^-): Synthesis and Application for Carbon Dioxide Reduction. *Polyhedron* **2017,** *125*, 156-163.

(54) Sheldrick, G. M., *Bruker/Siemens Area Detector Absorption Correction Program*. Bruker AXS, Madison, WI: 1998.

(55) Van der Sluis, P.; Spek, A. L., *Acta Cryst., Sect. A* **1990,** *A46*, 194-201.

(56) Sheldrick, G. M., *Acta Cryst.* **2015,** *C71*, 3-8.

TOC Image